Hindawi
Complexity
Volume 2022, Article ID 8238384, 14 pages
https://doi.org/10.1155/2022/8238384

WILEY | Hindawi

Research Article

Complex Dynamical Behavior of Holling–Tanner Predator-Prey Model with Cross-Diffusion

Caiyun Wang,[1] **Yongyong Pei**,[2] **Yaqun Niu**,[3] **and Ruiqiang He**[1]

[1]*Department of Mathematics, Xinzhou Teachers University, Xinzhou 034000, Shanxi, China*
[2]*The Affiliated Foreign Language Middle School of Xinzhou Teachers University, Xinzhou 034000, Shanxi, China*
[3]*Department of Mathematics, Taiyuan University, Taiyuan 034000, Shanxi, China*

Correspondence should be addressed to Caiyun Wang; 494423138@qq.com

Received 1 November 2021; Revised 26 November 2021; Accepted 15 December 2021; Published 10 January 2022

Academic Editor: Hiroki Sayama

Spatial predator-prey models have been studied by researchers for many years, because the exact distributions of the population can be well illustrated via pattern formation. In this paper, amplitude equations of a spatial Holling–Tanner predator-prey model are studied via multiple scale analysis. First, by amplitude equations, we obtain the corresponding intervals in which different kinds of patterns will be onset. Additionally, we get the conclusion that pattern transitions of the predator are induced by the increasing rate of conversion into predator biomass. Specifically, pattern transitions of the predator between distinct Turing pattern structures vary in an orderly manner: from spotted patterns to stripe patterns, and finally to black-eye patterns. Moreover, it is discovered that pattern transitions of prey can be induced by cross-diffusion; that is, patterns of prey transmit from spotted patterns to stripe patterns and finally to a mixture of spot and stripe patterns. Meanwhile, it is found that both effects of cross-diffusion and interaction between the prey and predator can lead to the complicated phenomenon of dynamics in the system of biology.

1. Introduction

Analysis of the dynamics of the predator-prey model is one of the most interesting topics in mathematics as well as in ecology. A variety of predator-prey models [1–7] that provide deep insight into the dynamical behaviors among interacting multiple species have already been investigated by many scholars in the past several decades. Pattern formation has already been analyzed in ecosystems [8–11] and epidemics for many years [12, 13]. In particular, pattern formation of the spatiotemporal predator-prey model has been avidly studied in recent decades [14–20] due to the following importance of the spatial patterns. First, the exact distributions of the population in both the spatial scale and time dimension can be well depicted by pattern formation. Second, further information on the evolution rules of individuals can be provided by spatial patterns. Finally, the influence of individual mobilities of one species on the other, such as stability and oscillatory dynamics, can be illustrated by spatial patterns.

One of the predator-prey models is Leslie predator-prey model which was first introduced by Leslie [21] and takes the form

$$\begin{cases} \dfrac{\mathrm{d}N}{\mathrm{d}\tau} = \phi(N)N - \psi(N)P, \\ \dfrac{\mathrm{d}P}{\mathrm{d}\tau} = \theta P\left(1 - \dfrac{hP}{N}\right), \end{cases} \tag{1}$$

where N and P stand for the population of prey and predator, respectively, at time τ. θ is the intrinsic growth rate of predator. h is the conversion factor of prey into predators. $\phi(N)$ describes the specific rate of the prey if there is no predator. $\psi(N)$ is the predator function response to prey. The predator's grow obeys logistic law, where the term N/h

means the carrying capacity of predator's environment which is proportional to the prey density. Robert May developed the Leslie predator-prey model by incorporating Holling type functional response [22, 23] to depict the predation rate. This model is known as Holling–Tanner model. Holling–Tanner model is suitable for ecological systems such as mite/spider mite, lynx/hare, sparrow/sparrow hawk, and so on [24–26]. In addition, it is assumed that the functional response is expressed by Holling type III response function [27, 28], i.e., $\psi(N) = mN^2P/aN^2 + 1$, which is more suitable for the population of vertebrates. When the prey grows logistically with growth rate r and carrying capacity K in the absence of predator, i.e., $\phi(N) = r(1 - N/K)$, we obtain the following Holling–Tanner model with Holling type III functional response:

$$\begin{cases} \dfrac{\mathrm{d}N}{\mathrm{d}\tau} = rN\left(1 - \dfrac{N}{K}\right) - \dfrac{mN^2P}{aN^2 + 1}, \\ \dfrac{\mathrm{d}P}{\mathrm{d}\tau} = \theta P\left(1 - \dfrac{hP}{N}\right), \end{cases} \tag{2}$$

where a is the half-saturation constant. m is the maximum number of the prey that predator can capture per unit time.

It is well known that spatial motion in predator–prey models includes both self-diffusion and cross-diffusion. Self-diffusion denotes the random individual mobility and indicates the movement of individuals from a higher- to lower-concentration region [29]. The concept of cross-diffusion was first proposed by Kerner [30] and was then introduced into the competitive species system [31, 32]. Taking the prey–predator model as an example, cross-diffusion terms explain the following biological meaning: predator species will move towards various directions and affect the density of different prey species at distinct places, and vice versa [33]. The mutual migration among species is typical cross-diffusion. Several phenomena cannot be well explained by only incorporating the self-diffusion term [34]; for example, there is no Turing instability in the Lotka–Volterra competitive model when only self-diffusion has been incorporated. Once the cross-diffusion term is taken into account, the above model can induce Turing instability under certain conditions. Numerous works are relevant to spatial motion [35–40]. Peng R demonstrated that cross-diffusion can induce stationary effects [41]. Oeda studied a predator-prey model with cross-diffusion and proposed a protection zone for the prey and concluded that the prey will survive because of the benefits of effects of cross-diffusion on the prey when several conditions are satisfied [42]. An attempt is made in this paper to understand the effect of cross-diffusion on the prey-predator model as well.

It is clear that both intrinsic interaction between the prey and predator and the cross-diffusion affect the dynamics of the population in the predator-prey model with cross-diffusion. Our aim is to explore such effects. Moreover, most predator-prey models are nonlinear systems in order to reflect the real world [43, 44]. The nonlinear system should be approximated more accurately than in linear stability analysis. Based on Q. Ouyang's work [45], multiple scale analysis is used to study a ratio-dependent predator-prey model with spatial motion in the present paper. Let N and P stand for the density of the prey and predator, respectively. The model is expressed as

$$\begin{cases} \dfrac{\partial N}{\partial \tau} = rN\left(1 - \dfrac{N}{K}\right) - \dfrac{mN^2P}{aN^2 + 1} + D_{11}\nabla^2 N + D_{12}\nabla^2 P, \quad (y, \tau) \in \Omega \times (0, \infty), \\ \dfrac{\partial P}{\partial \tau} = \theta P\left(1 - \dfrac{hP}{N}\right) + D_{21}\nabla^2 N + D_{22}\nabla^2 P, \quad (y, \tau) \in \Omega \times (0, \infty), \\ \dfrac{\partial N(y, \tau)}{\partial n} = \dfrac{\partial P(y, \tau)}{\partial n} = 0, \quad (y, \tau) \in \partial\Omega \times (0, \infty), \\ N(y, 0) = N_0 > 0, \quad y \in \Omega, \\ P(y, 0) = P_0 > 0, \quad y \in \Omega, \end{cases} \tag{3}$$

where Ω represents the bounded domain in R^2, and $\partial\Omega$ is the smooth bound of Ω with n being its external unit normal vector. The meanings and values of the parameters are given in Table 1.

Introducing the dimensionless variables $u = N/K$, $v = mKP/r$, and $t = r\tau$, then system (3) can be transformed into

Table 1: The meaning of parameters in model (3).

Parameter	Value	Meaning
r	Positive	Prey's intrinsic growth rate
m	Positive	Capturing rate
a	Positive	Half-saturation constant
θ	Positive	Predator's intrinsic growth rate
K	Positive	Carrying capacity
h	Positive	Conversion rate of biomass from prey to predator
D_{11}	Positive	Diffusion coefficient of prey
D_{22}	Positive	Diffusion coefficient predator
D_{12}	Negative	Cross-diffusion coefficient of prey
D_{21}	Positive	Cross-diffusion coefficient of predator

$$\begin{cases} \dfrac{\partial u}{\partial t} = u(1-u) - \dfrac{u^2 v}{eu^2+v} + d_{11}\nabla^2 u + d_{12}\nabla^2 v, \quad (y,t) \in \Omega \times (0,\infty), \\ \dfrac{\partial v}{\partial t} = v\eta\left(1 - \dfrac{\gamma v}{u}\right) + d_{21}\nabla^2 u + d_{22}\nabla^2 v, \quad (y,t) \in \Omega \times (0,\infty), \\ \dfrac{\partial u(y,t)}{\partial n} = \dfrac{\partial v(y,t)}{\partial n} = 0, \quad (y,t) \in \partial\Omega \times (0,\infty), \\ u(y,0) = u_0 > 0, \quad y \in \Omega, \\ v(y,0) = v_0 > 0, \quad y \in \Omega, \end{cases} \tag{4}$$

where $\eta = \theta/r, e = aK^2, \gamma = hr/mK^2, d_{11} = \mathrm{KD}_{11}/r, d_{12} = rD_{12}/m^2K^3, d_{21} = mK^3D_{21}/r^2$, and $d_{22} = D_{22}/mK$.

The rest of this paper is organized as follows. In Section 2, several conditions for the onset of the Turing instability are derived by bifurcation analysis. To show the results, an example is also provided. In Section 3, the amplitude equations near the Turing bifurcation point are obtained by virtue of weakly nonlinear analysis. To illustrate the theoretical analysis, a numerical simulation is conducted in Section 4. Moreover, pattern transitions of both the predator induced by parameter γ and prey induced by parameter d_{12} are obtained by simulations. Pattern transitions are obtained both by the biomass from prey to predator and by the cross-diffusion of the prey. The results reveal the complicated mutual effects of cross-diffusion and the intrinsic mechanism, e.g., biomass on the predator-prey system.

2. Bifurcation Analysis

We will show the Turing domain through bifurcation analysis in this section; for details of linear stability analysis of the existence, local stability, and the types of the positive equilibrium of model (4), the reader is referred to [46], while in the following, a concrete example is given to show the existence and stability of positive equilibrium. For convenience, let

$$u(1-u) - \frac{u^2 v}{eu^2+1} \triangleq f(u,v), \quad v\eta\left(1 - \frac{\gamma v}{u}\right) \triangleq g(u,v). \tag{5}$$

Without loss of generality, let $E^*(u^*, v^*)$ be the positive equilibrium of model (4). System (4) can be linearized at $E^*(u^*, v^*)$,

$$\frac{\partial \widehat{A}}{\partial t} = J\widehat{A} + \mathrm{DL}\widehat{A}, \tag{6}$$

where

$$\widehat{A} = \begin{pmatrix} u - u^* \\ v - v^* \end{pmatrix}, \quad J = \begin{pmatrix} f_u & f_v \\ g_u & g_v \end{pmatrix}, \quad D = \begin{pmatrix} d_{11} & d_{12} \\ d_{21} & d_{22} \end{pmatrix}, \quad L = \begin{pmatrix} \nabla^2 & \nabla^2 \\ \nabla^2 & \nabla^2 \end{pmatrix}, \tag{7}$$

where

$$f_u = \frac{-2e(u^*)^3 + e(u^*)^2 - 1}{e(u^*)^2 + 1}, \quad f_v = \frac{-(u^*)^2}{e(u^*)^2 + 1}, \quad g_u = \frac{\eta}{\gamma}, \quad g_v = -\eta, \tag{8}$$

and obviously,

$$tr(J) = f_u + g_v, \quad \det(J) = f_u g_v - f_v g_u. \tag{9}$$

We will give a concrete value of the equilibrium $E^*(u^*, v^*)$ as an example of the existence and stability of the equilibrium with the other values of parameters shown in Table 2.

Next, expand $\widehat{A}$ in Fourier space, that is, substituting

$$\widehat{A} = \begin{pmatrix} c_k^1 \\ c_k^2 \end{pmatrix} e^{\lambda_k t + ik\cdot r}, \tag{10}$$

into (6), where $k = (k_x, k_y)$, $r = (x, y)$. Following characteristic equation is obtained:

$$\lambda_k^2 - tr_k \lambda_k + \Delta_k = 0, \tag{11}$$

where

$$\begin{aligned} tr_k &= (f_u + g_v) - k^2(d_{11} + d_{22}), \\ \Delta_k &= f_u g_v - f_v g_u - k^2[d_{22} f_u + d_{11} g_v - (d_{12} g_u + d_{21} f_v)] \\ &\quad + (d_{11} d_{22} - d_{12} d_{21})k^4, \end{aligned} \tag{12}$$

and the eigenvalue of (11) is given as

$$\lambda_k = \frac{tr_k \pm \sqrt{tr_k^2 - 4\Delta_k}}{2}. \tag{13}$$

Table 2: A concrete example to illustrate the existence and stability of the equilibrium $E^*(u^*, v^*)$.

η	γ	e	u^*	v^*	$tr(J)$	$\det(J)$
0.5	0.001455604076	900	0.25	171.75	−0.026008734	0.1381004367

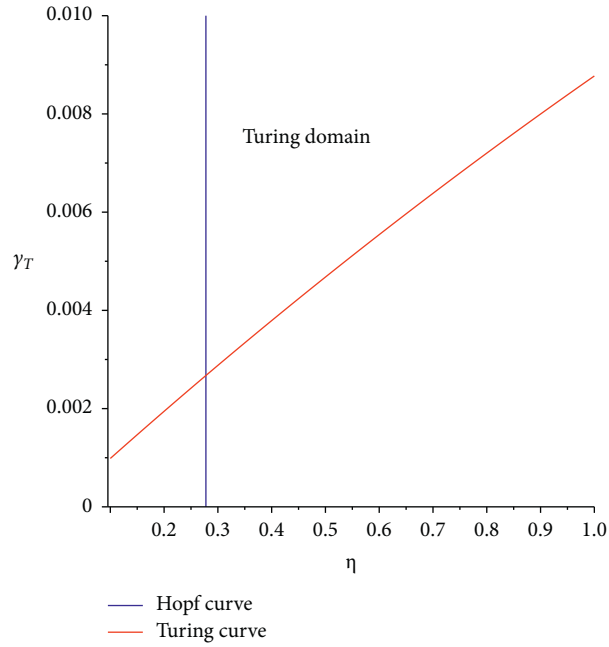

Figure 1: Turing domain of model (4).

Hopf bifurcation occurs when the conditions $\mathrm{Re}(\lambda_k) = 0$, $\mathrm{Im}(\lambda_k) \neq 0$, $tr(J) = 0$, and $\det(J) > 0$, at $k = 0$, are satisfied. When conditions such as $\mathrm{Re}(\lambda_k) = 0$ and $\mathrm{Im}(\lambda_k) = 0$, which require $\Delta_k = 0$ at $k = k_T$, are satisfied, Turing bifurcation appears, and

$$k_T^2 = \sqrt{\frac{f_u g_v - f_v g_u}{d_{11}d_{22} - d_{12}d_{21}}}. \tag{14}$$

Substituting (14) into $\Delta_K = 0$, the expression of γ_T, the value of which is the critical value for the appearance of Turing bifurcation, is obtained:

$$\gamma_T = \frac{\left(\left(\begin{array}{c} -d_{11}d_{12}\eta u^2 e - 2d_{12}d_{22}u^3 e + d_{12}d_{22}u^2 e + 2d_{11}d_{22}u^2 - d_{12}d_{21}u^2 - d_{11}d_{12}\eta - d_{12}d_{22} + \\ 2d_{11}d_{12}^2 e^2 \eta u^5 d_{22} - 2d_{12}^3 e^2 \eta u^5 d_{21} - d_{11}d_{12}^2 e^2 \eta u^4 d_{22} + d_{12}^3 e^2 \eta u^4 d_{21} - d_{11}^2 d_{12} e \eta u^4 d_{22} \\ + d_{11}d_{12}^2 e \eta u^4 d_{21} - 2d_{11}d_{12} e u^5 d_{22}^2 + 2d_{11}d_{12}^2 e \eta u^3 d_{22} + d_{11}d_{12} e u^4 d_{22}^2 - 2d_{12}^3 e \eta u^3 d_{21} - \\ d_{12}^2 e u^4 d_{21} d_{22} + 2d_{12} e u^5 d_{21} d_{22} + d_{11}^2 u^4 d_{22}^2 - d_{11}d_{12}u^4 d_{21}d_{22} - d_{11}^2 d_{12}\eta u^2 d_{22} + d_{11}d_{12}^2 \eta u^2 d_{21} - \\ d_{11}d_{12}u^2 d_{22}^2 + d_{12}^2 u^2 d_{21}d_{22} + d_{11}d_{12}^2 \eta d_{22} - d_{12}^3 \eta d_{21} \end{array}\right)^{1/2}\right)\eta\left(eu^2 + 1\right)\right)}{\left(\begin{array}{c} d_{11}^2 e^2 u^4 \eta^2 - 4d_{11}e^2 \eta u^5 d_{22} + 8d_{12}\eta u^5 \varepsilon^2 d_{21} + 4e^2 u^6 d_{22}^2 + \\ 2d_{11}e^2 \eta u^4 d_{22} - 4d_{12}e^2 \eta u^4 d_{21} - 4e^2 u^5 d_{22}^2 - 2d_{11}e\eta u^4 d_{21} + e^2 u^4 d_{22}^2 - 4eu^5 d_{21}d_{22} + \\ 2d_{11}^2 e\eta^2 u^2 - 4d_{11}e\eta u^3 d_{22} + 8d_{12}e\eta u^3 d_{21} + 2eu^4 d_{21}d_{22} + 4eu^3 d_{22}^2 + u^4 d_{21}^2 - \\ 2d_{11}\eta u^2 d_{21} - 2eu^2 d_{22}^2 + d_{11}^2 \eta^2 - 2u^2 d_{21}d_{22} - 2d_{11}\eta d_{22} + 4d_{12}\eta d_{21} + d_{22}^2 \end{array}\right)}. \tag{15}$$

When the values of the parameters are set as $\eta = 0.8$, $e = 130$, $d_{11} = 0.1$, $d_{22} = 8.5$, $d_{12} = 0.008$, and $d_{21} = -0.08$, let Turing domain denote the area where Turing patterns will be observed. Turing domain and the real part of λ_k of model (4) can be plotted as shown in Figure 1 and Figure 2, respectively.

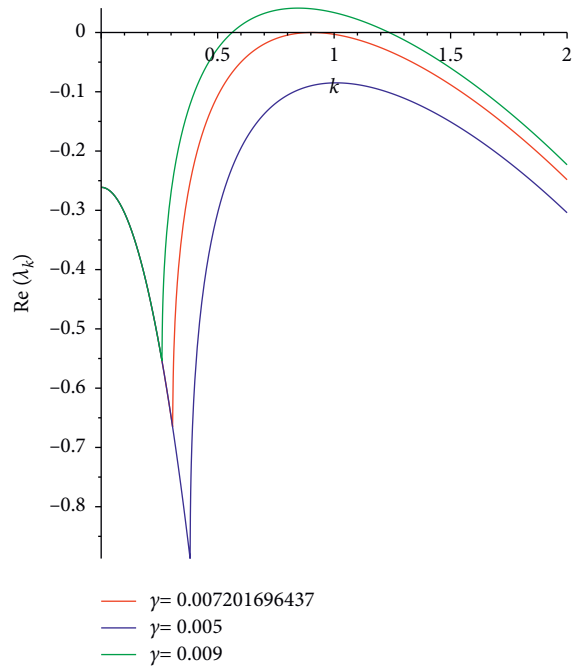

Figure 2: Dispersion relation of system (4), which shows the real part of eigenvalues λ_k of model (4).

3. Multiple Scale Analysis

To obtain the intervals of the control parameter for different types of patterns, the amplitude equations for Turing patterns of system (4) are analyzed via multiple scale analysis [45, 47] near the branch point in this section, with γ and γ_T being the control parameter and bifurcation threshold, respectively. Near $\gamma = \gamma_T$, the solution of system (4) is

$$\begin{pmatrix} u \\ v \end{pmatrix} = \sum_{j=1}^{3} \begin{pmatrix} A_j^u \\ A_j^v \end{pmatrix} e^{ik_j \cdot r} + c.c \ldots, \tag{16}$$

where $|k_j| = k_T$, A_j^u, A_j^v stand for the amplitude of the pattern, and $c.c$stands for the conjugate item.

$$\sum_{j=1}^{3} \begin{pmatrix} \overline{A}_j^u \\ \overline{A}_j^v \end{pmatrix} e^{-ik_j \cdot r}. \tag{17}$$

System (4) can be written at $E^*(u^*, v^*)$ as

$$\frac{\partial X}{\partial t} = \mathrm{L}X + \widetilde{N}, \tag{18}$$

where

$$L = \begin{pmatrix} f_u + d_{11}\nabla^2 & f_v + d_{12}\nabla^2 \\ g_u + d_{21}\nabla^2 & g_v + d_{22}\nabla^2 \end{pmatrix},$$

$$\widetilde{N} = \begin{pmatrix} \frac{1}{6}f_{111}u^3 + \frac{1}{6}f_{222}v^3 + \frac{1}{6}(f_{112} + f_{121} + f_{211})u^2v + \frac{1}{6}(f_{122} + f_{212} + f_{221})uv^2 + \frac{1}{2}(f_{12} + f_{21})uv + \frac{1}{2}f_{11}u^2 + \frac{1}{2}f_{22}v^2 \\ \frac{1}{6}g_{111}u^3 + \frac{1}{6}g_{222}v^3 + \frac{1}{6}(g_{112} + g_{121} + g_{211})u^2v + \frac{1}{6}(g_{122} + g_{212} + g_{221})uv^2 + \frac{1}{2}(g_{12} + g_{21})uv + \frac{1}{2}g_{11}u^2 + \frac{1}{2}g_{22}v^2 \end{pmatrix}. \tag{19}$$

γ, X, t, and N then can be expanded around the threshold γ_T as follows. The specific expressions of h_2 and h_3 are

$$\begin{aligned}
&\gamma_T - \gamma = \varepsilon\gamma_1 + \varepsilon^2\gamma_2 + \ldots,\\
&X = \begin{pmatrix} u \\ v \end{pmatrix} = \varepsilon\begin{pmatrix} u_1 \\ v_1 \end{pmatrix} + \varepsilon^2\begin{pmatrix} u_2 \\ v_2 \end{pmatrix} + \varepsilon^3\begin{pmatrix} u_3 \\ v_3 \end{pmatrix} + o\left(\varepsilon^4\right),\\
&t = T_0 + \varepsilon T_1 + \varepsilon^2 T_2,\\
&\widetilde{N} = \varepsilon^2 h_2 + \varepsilon^3 h_3 + o\left(\varepsilon^4\right),
\end{aligned} \tag{20}$$

where the specific expressions of h_2 and h_3 are

$$h_2 = \begin{pmatrix} \frac{1}{2}f_{11}u_1^2 + \frac{1}{2}(f_{12} + f_{21})u_1v_1 + \frac{1}{2}f_{22}v_1^2 \\ \frac{1}{2}g_{11}u_1^2 + \frac{1}{2}(g_{12} + g_{21})u_1v_1 + \frac{1}{2}g_{22}v_1^2 \end{pmatrix}, \tag{21}$$

$$h_3 = \begin{pmatrix} \frac{1}{6}f_{111}u_1^3 + \frac{1}{6}f_{222}v_1^3 + \frac{1}{6}(f_{112} + f_{121} + f_{211})u_1^2v_1 + \frac{1}{6}(f_{122} + f_{212} + f_{221})u_1v_1^2 + f_{11}u_2u_1 + f_{22}v_2v_1 + \frac{1}{2}(f_{12} + f_{21})(u_2v_1 + u_1v_2) \\ \frac{1}{6}g_{111}u_1^3 + \frac{1}{6}g_{222}v_1^3 + \frac{1}{6}(g_{112} + g_{121} + g_{211})u_1^2v_1 + \frac{1}{6}(g_{122} + g_{212} + g_{221})u_1v_1^2 + g_{11}u_2u_1 + g_{22}v_2v_1 + \frac{1}{2}g_{12} + g_{21}\Big)(u_2v_1 + u_1v_2) \end{pmatrix}.$$

Meanwhile, the operator L can be expanded by Taylor expansion and can be written as

$$L = L_T + (\gamma_T - \gamma)M, \tag{22}$$

where

$$\begin{aligned}
&L_T = \begin{pmatrix} f_u + d_{11}\nabla^2 & f_v + d_{12}\nabla^2 \\ g_u^* + d_{21}\nabla^2 & g_v + d_{22}\nabla^2 \end{pmatrix},\\
&g_u^* = \frac{\eta}{\gamma_T},\\
&M = \begin{pmatrix} 0 & 0 \\ \frac{\eta}{\gamma_T^2} & 0 \end{pmatrix}.
\end{aligned} \tag{23}$$

Let

$$A^j = \begin{pmatrix} A_j^u \\ A_j^v \end{pmatrix}. \tag{24}$$

$\partial A^j/\partial T_0 = 0$ is satisfied, because the amplitude is a slow variable. For the derivation of the amplitude, one has

$$\frac{\partial A^j}{\partial t} = \varepsilon\frac{\partial A^j}{\partial T_1} + \varepsilon^2\frac{\partial A^j}{\partial T_2} + \ldots. \tag{25}$$

Substituting (20)–(25) into (18) and collecting $\varepsilon, \varepsilon^2$, and ε^3, one has the linear systems ε:

$$L_T\begin{pmatrix} u_1 \\ v_1 \end{pmatrix} = 0. \tag{26}$$

ε^2:

$$L_T\begin{pmatrix} u_2 \\ v_2 \end{pmatrix} = \frac{\partial}{\partial T_1}\begin{pmatrix} u_1 \\ v_1 \end{pmatrix} - d_{11}M\begin{pmatrix} u_1 \\ v_1 \end{pmatrix} - h_2 \triangleq \begin{pmatrix} F_u \\ F_v \end{pmatrix}. \tag{27}$$

ε^3:

$$\begin{aligned}
L_T\begin{pmatrix} u_3 \\ v_3 \end{pmatrix} &= \frac{\partial}{\partial T_1}\begin{pmatrix} u_2 \\ v_2 \end{pmatrix} + \frac{\partial}{\partial T_2}\begin{pmatrix} u_1 \\ v_1 \end{pmatrix} - d_{11}M\begin{pmatrix} u_2 \\ v_2 \end{pmatrix}\\
&\quad - d_{22}M\begin{pmatrix} u_1 \\ v_1 \end{pmatrix} - h_3 \triangleq \begin{pmatrix} H_u \\ H_v \end{pmatrix},
\end{aligned} \tag{28}$$

where

$$\begin{pmatrix} F_u \\ F_v \end{pmatrix} = \sum_{j=1}^{3}\begin{pmatrix} F_u^j \\ F_v^j \end{pmatrix}e^{ik_j\cdot r} + c.c.. \tag{29}$$

$$\begin{pmatrix} H_u \\ H_v \end{pmatrix} = \sum_{j=1}^{3}\begin{pmatrix} H_u^j \\ H_v^j \end{pmatrix}e^{ik_j\cdot r} + c.c.. \tag{30}$$

Solving equation (26) in the light of [36] one obtains the solution of equation (26):

$$\begin{pmatrix} u_1 \\ v_1 \end{pmatrix} = \begin{pmatrix} l \\ 1 \end{pmatrix}\left[W_1 e^{ik_1\cdot r} + W_2 e^{ik_2\cdot r} + W_3 e^{ik_3\cdot r}\right] + c.c., \quad (31)$$

where $l = d_{12}k_T^2 - f_v/f_u - d_{11}k_T^2$, $c.c$denotes complex conjugate, and $W_i\,(i = 1, 2, 3)$ is the amplitude of the pattern for the first-order perturbation with mode $e^{i\mathbf{k}_j\cdot\mathbf{r}}$, the form of which is determined by higher-order terms.

On the basis of the Fredholm solvability condition, (31) is substituted into equation (27) to obtain the eigenvector of the operator of L_T^+,

$$\begin{pmatrix} 1 \\ l_2 \end{pmatrix} e^{-ik_j\cdot r} + c.c., \quad (j = 1, 2, 3), \quad (32)$$

where L_T^+ is the eigenvector of the zero eigenvalue of the adjoint operator of L_T, and

$$l_2 = \frac{k_T^2 d_{12} - f_v}{g_v - d_{22}k_T^2}. \quad (33)$$

The orthogonality condition is given by

$$(1, l_2)\begin{pmatrix} F_u^i \\ F_v^i \end{pmatrix} = 0\,(i = 1, 2, 3), \quad (34)$$

and from (34), the following equalities are given:

$$\begin{cases} (l + l_2)\dfrac{\partial W_1}{\partial T_1} = \gamma_1 l_2 l\dfrac{\eta}{\gamma_T^2}W_1 + \left[f_{11}l^2 + (f_{12} + f_{21})l + f_{22} + l_2\left(g_{11}^* l^2 + (g_{12}^* + g_{21}^*)l + g_{22}^*\right)\right]\overline{W}_2\overline{W}_3, \\ (l + l_2)\dfrac{\partial W_2}{\partial T_1} = \gamma_1 l_2 l\dfrac{\eta}{\gamma_T^2}W_2 + \left[f_{11}l^2 + (f_{12} + f_{21})l + f_{22} + l_2\left(g_{11}^* l^2 + (g_{12}^* + g_{21}^*)l + g_{22}^*\right)\right]\overline{W}_1\overline{W}_3, \\ (l + l_2)\dfrac{\partial W_3}{\partial T_1} = \gamma_1 l_2 l\dfrac{\eta}{\gamma_T^2}W_3 + \left[f_{11}l^2 + (f_{12} + f_{21})l + f_{22} + l_2\left(g_{11}^* l^2 + (g_{12}^* + g_{21}^*)l + g_{22}^*\right)\right]\overline{W}_1\overline{W}_2, \end{cases} \quad (35)$$

where g_{ij}^* denotes the outcome of γ in g_{ij} replaced by γ_T .

Assume that the following expression is the solution of equation (27),

$$\begin{pmatrix} u_2 \\ v_2 \end{pmatrix} = \begin{pmatrix} U_0 \\ V_0 \end{pmatrix} + \sum_{j=1}^{3}\begin{pmatrix} U_j \\ V_j \end{pmatrix} e^{ik_j\cdot r} + \sum_{j=1}^{3}\begin{pmatrix} U_{jj} \\ V_{jj} \end{pmatrix} e^{i2k_j\cdot r} + \begin{pmatrix} U_{12} \\ V_{12} \end{pmatrix} e^{i(k_1 - k_2)\cdot r} + \begin{pmatrix} U_{23} \\ V_{23} \end{pmatrix} e^{i(k_2 - k_3)\cdot r} + \begin{pmatrix} U_{31} \\ V_{31} \end{pmatrix} e^{i(k_1 - k_1)\cdot r} + c.c.,. \quad (36)$$

Substituting (36) into (27) and collecting the coefficients of $\exp(0)$, $\exp(ik_j\cdot r)$, $\exp(i2k_j\cdot r)$, and $\exp(i(k_j - k_i)\cdot r)$, the following expressions are obtained:

$$\begin{aligned} \begin{pmatrix} U_0 \\ V_0 \end{pmatrix} &= \begin{pmatrix} u_0 \\ v_0 \end{pmatrix}\left(|W_1|^2 + |W_2|^2 + |W_3|^2\right), \\ U_j &= lV_j, \\ \begin{pmatrix} U_{jj} \\ V_{ij} \end{pmatrix} &== \begin{pmatrix} u_{11} \\ v_{11} \end{pmatrix} W_j^2, \\ \begin{pmatrix} U_{mn} \\ V_{mn} \end{pmatrix} &= \begin{pmatrix} u_{mn} \\ v_{mn} \end{pmatrix} W_m\overline{W}_n, \end{aligned} \quad (37)$$

where

$$\begin{pmatrix} u_0 \\ v_0 \end{pmatrix} = \frac{1}{f_u g_v - f_v g_u^*}\cdot\begin{pmatrix} -g_v\left(f_{11}l^2 + (f_{12} + f_{21})l + f_{22}\right) + f_v\left(g_{11}^* l^2 + (g_{12}^* + g_{21}^*)l + g_{22}^*\right) \\ -f_u\left(g_{11}^* l^2 + (g_{12}^* + g_{21}^*)l + g_{22}^*\right) + g_u^*\left(f_{11}l^2 + (f_{12} + f_{21})l + f_{22}\right) \end{pmatrix},$$

$$\begin{pmatrix} u_{11} \\ v_{11} \end{pmatrix} = \frac{1}{2}\cdot\frac{1}{\left(f_u - 4k_T^2 d_{11}\right)\left(g_v - 4k_T^2 d_{22}\right) - \left(f_v - 4k_T^2 d_{12}\right)\left(g_u^* - 4k_T^2 d_{21}\right)}\cdot\begin{pmatrix} -\left(g_v - 4K_T^2 d_{22}\right)\left(f_{11}l^2 + (f_{12} + f_{21})l + f_{22}\right) + \left(f_v - 4k_T^2 d_{12}\right)\left(g_{11}^* l^2 + (g_{12}^* + g_{21}^*)l + g_{22}^*\right) \\ -\left(f_u - 4k_T^2 d_{11}\right)\left(g_{11}^* l^2 + (g_{12}^* + g_{21}^*)l + g_{22}^*\right) + \left(g_u^* - 4k_T^2 d_{21}\right)\left(f_{11}l^2 + (f_{12} + f_{21})l + f_{22}\right) \end{pmatrix},$$

$$\begin{pmatrix} u_m \\ v_{mn} \end{pmatrix} = \frac{1}{\left(f_u - 4k_T^2 d_{11}\right)\left(g_v - 4k_T^2 d_{22}\right) - \left(f_v - 4k_T^2 d_{12}\right)\left(g_u^* - 4k_T^2 d_{21}\right)}\cdot\begin{pmatrix} -\left(g_v - 4K_T^2 d_{22}\right)\left(f_{11}l^2 + (f_{12} + f_{21})l + f_{22}\right) + \left(f_v - 4k_T^2 d_{12}\right)\left(g_{11}^* l^2 + (g_{12}^* + g_{21}^*)l + g_{22}^*\right) \\ -\left(f_u - 4k_T^2 d_{11}\right)\left(g_{11}^* l^2 + (g_{12}^* + g_{21}^*)l + g_{22}^*\right) + \left(g_u^* - 4k_T^2 d_{21}\right)\left(f_{11}l^2 + (f_{12} + f_{21})l + f_{22}\right) \end{pmatrix}. \quad (38)$$

Using the Fredholm solvability condition, one obtains

$$(1, l_2)\begin{pmatrix} H_u^j \\ H_v^j \end{pmatrix} = 0\,(j = 1, 2, 3). \tag{39}$$

Equation (39) yields

$$\begin{cases} (l+l_2)\left(\dfrac{\partial V_1}{\partial T_1}+\dfrac{\partial W_1}{\partial T_2}\right) = ll_2\dfrac{\eta}{\gamma_T^2}(\gamma_1 V_1+\gamma_2 W_1)+\widetilde{A}(\overline{V}_2\overline{W}_3+\overline{V}_3\overline{W}_2)+\left(B_1|W_1|^2+B_2\left(|W_2|^2+|W_3|^2\right)\right)W_1, \\ (l+l_2)\left(\dfrac{\partial V_2}{\partial T_1}+\dfrac{\partial W_2}{\partial T_2}\right) = ll_2\dfrac{\eta}{\gamma_T^2}(\gamma_1 V_2+\gamma_2 W_2)+\widetilde{A}(\overline{V}_1\overline{W}_3+\overline{V}_3\overline{W}_1)+\left(B_1|W_2|^2+B_2\left(|W_1|^2+|W_3|^2\right)\right)W_2, \\ (l+l_2)\left(\dfrac{\partial V_3}{\partial T_1}+\dfrac{\partial W_3}{\partial T_2}\right) = ll_2\dfrac{\eta}{\gamma_T^2}(\gamma_1 V_3+\gamma_2 W_3)+\widetilde{A}(\overline{V}_1\overline{W}_2+\overline{V}_2\overline{W}_1)+\left(B_1|W_3|^2+B_2\left(|W_1|^2+|W_2|^2\right)\right)W_3, \end{cases} \tag{40}$$

where

$$\begin{aligned} &\widetilde{A} = (lm_1+n_1)+l_2(lm_2+n_2), \\ &B_1 = \left(am_1+a_1n_1+\frac{P_1}{2}\right)+l_2\left(am_2+a_1n_2+\frac{P_2}{2}\right), \\ &B_2 = (bm_1+b_1n_1+P_1)+l_2(bm_2+b_1n_2+P_2), \\ &a = u_0+u_{11},\quad b = u_0+u_{mn}, \\ &a_1 = v_0+v_{11},\quad b_1 = v_0+v_{mn}, \\ &m_1 = f_{11}l+\frac{1}{2}(f_{12}+f_{21}),\quad n_1 = f_{22}+\frac{1}{2}(f_{12}+f_{21})l, \\ &m_2 = g_{11}^*l+\frac{1}{2}(g_{12}^*+g_{21}^*),\quad n_2 = g_{22}^*+\frac{1}{2}(g_{12}^*+g_{21}^*)l, \\ &P_1 = f_{111}l^3+(f_{112}+f_{121}+f_{211})l^2+(f_{122}+f_{212}+f_{221})l+f_{222}, \\ &P_2 = g_{111}^*l^3+(g_{112}^*+g_{121}^*+g_{211}^*)l^2+(g_{122}^*+g_{212}^*+g_{221}^*)l+g_{222}, \end{aligned} \tag{41}$$

where g_{ijk}^* denotes the outcome of γ in g_{ijk} replaced by γ_T.

Through the above expression, together with (13) and the following formula

$$A_i = A_i^u = \mathrm{LA}_i^v,\quad (i = 1, 2, 3), \tag{42}$$

one has the amplitude equations for patterns of system (4):

$$\begin{cases} \tau_0\dfrac{\partial A_1}{\partial t} = \mu A_1+h\overline{A}_2\overline{A}_3-\left(g_1|A_1|^2+g_2\left(|A_2|^2+|A_3|^2\right)\right)A_1, \\ \tau_0\dfrac{\partial A_2}{\partial t} = \mu A_2+h\overline{A}_1\overline{A}_3-\left(g_1|A_2|^2+g_2\left(|A_1|^2+|A_3|^2\right)\right)A_2, \\ \tau_0\dfrac{\partial A_3}{\partial t} = \mu A_3+h\overline{A}_1\overline{A}_2-\left(g_1|A_3|^2+g_2\left(|A_1|^2+|A_2|^2\right)\right)A_3, \end{cases} \tag{43}$$

where

$$\begin{aligned} \tau_0 &= \frac{(l+l_2)\gamma_T}{ll_2\eta}, \\ \mu &= \frac{\gamma_1^T-\gamma_1}{\gamma_T}, \\ h &= \frac{A\gamma_T}{l^2l_2\eta}, \\ g_1 &= -\frac{B_1\gamma_T}{l^3l_2\eta}, \\ g_2 &= -\frac{B_2\gamma_T}{l^3l_2\eta}. \end{aligned} \tag{44}$$

Based on [45] and the above analysis, we get the intervals for the pattern selection, i.e., the corresponding intervals for different kinds of pattern being observed. The results presented in Table 3 are obtained.

4. Numerical Simulations of Patterns

In this section, the value of γ is chosen and numerical simulations are performed to verify the theoretical results. Model (4) is simulated via a finite difference approximation for spatial derivatives and the Euler method is employed. The zero-flux boundary condition with 200×200 lattice sites is employed, and the space step $\Delta h = 1$ and time step $\Delta t = 0.01$ are set. The simulation is run until the pattern features no longer vary. For the similar distributions on prey and predator, the predator's pattern is chosen to illustrate details of the investigation.

4.1. Selection of the Predator's Pattern. The aim here is to verify the theoretical analysis presented in Section 3 and determine whether the patterns arise in their corresponding Turing domains as given in the preceding section. First, the other parameters in system (4), shown in Table 4, are fixed and the value of γ is varied. The values of parameters in amplitude equation (43) are then calculated in Table 5.

Table 3: Pattern selection of model (4).

μ	Pattern	Stability
$\mu_2 < \mu = 0.0068256080 < \mu_3$	H_π spot pattern	Unstable
$\mu_2 < \mu = 0.0290608556 < \mu_3$	Mixture of cold spots and stripe patterns	Unstable
$\mu_2 < \mu = 0.1031783475 < \mu_3$	Stripe pattern	Unstable
$\mu_3 < \mu = 0.1254135951 < \mu_4$	Mixture of hot spots and stripe patterns	Bistable
$\mu_3 < \mu = 0.2217663346 < \mu_4$	H_0 spot pattern	Unstable

Table 4: Parameters set in system (4).

η	e	d_{11}	d_{22}	d_{12}	d_{21}
1.4	100	0.123	12	0.006	−0.07

Table 5: Parameters calculated in system (4).

γ_T	g_1	g_2	h	μ_1	μ_2	μ_3	μ_4
0.013492091 73	11.852514 87	71.487989 95	5.892541 152	−0.05606532777	0	0.115719457 9	0.929 39

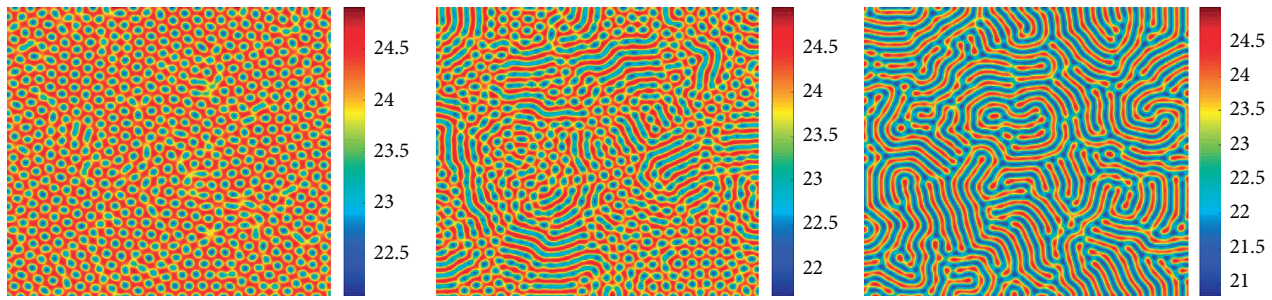

Figure 3: Unstable spot pattern, mixture of spots and stripes patterns, and stripe pattern of the predator. Other parameters are set as in Table 4, and (a) $\gamma = 0.0134$, (b) $\gamma = 0.0131$, and (c) $\gamma = 0.0121$.

For $\gamma = 0.0134$, one has $\mu_2 < \mu = 0.0068256080 < \mu_3$. On the basis of the results obtained in Section 3, the unstable spot pattern H_π of the predator is obtained as shown in Figure 3(a). To show the instability of the H_π spot pattern, by changing the value of γ slightly, namely, $\gamma = 0.0131$ and $\gamma = 0.0121$, where $\mu_2 < \mu = 0.0290608556 < \mu_3$ and $\mu_2 < \mu = 0.1031783475 < \mu_3$, it can be seen from Figure 3 that spot pattern H_π turns into an unstable mixture of cold spots and stripe patterns in Figure 3(b) and stripe pattern in Figure 3(c). This mathematical analysis is consistent with numerical simulation.

For $\gamma = 0.0118, \mu_3 < \mu = 0.1254135951 < \mu_4$, in light of the results presented in Table 3, a stable mixture of a hot spots and stripes pattern is obtained. Figure 4 shows the evolution of the mixture of hot spots and stripes of the predator. The numerical simulation verifies the theoretical analysis. Moreover, when $\gamma = 0.0105$ is chosen, corresponding to $\mu_3 < \mu = 0.2217663346 < \mu_4$, the H_0 spot pattern is obtained. Figure 5 shows the iterations of the hot spot pattern.

4.2. Pattern Transitions of the Predator Induced by Parameter γ. In this subsection, how the spatial distribution of the predator transforms as the conversion rate of the prey into predator biomass changes is investigated. The values of the other parameters are set in Table 6, and the value of γ is increased gradually. Specifically, when γ is set as $\gamma = 0.007041633659$, the hot spot pattern will dominate the entire spatial region in Figure 6(a). In Figure 6(b), when $\gamma = 0.008509501103$ is chosen, then the mixture of hot spots and stripes arises. When γ increases to 0.009 332 994 621, only a stripe pattern can be simulated in Figure 6(c). When γ grows further to $\gamma = 0.01032204568$, the mixture of cold spots and stripes occurs as shown in Figure 6(d). Finally, when γ becomes even larger, i.e., $\gamma = 0.01092704597$, the cold spot pattern shown in Figure 6(e) manifests. Figure 6 shows not only the regular changes of the pattern transition, but also that the density of the predator increases from 31 to 31.5 gradually as the γ value increases. Since γ is the amount of the prey captured by every predator, the larger the value of parameter γ, the more food the predator will eat. From the biological perspective, the more food the predator eats, the larger the predator population will be. In other words, our results are consistent with the real case in the ecosystem.

4.3. Pattern Transitions of Prey Induced by Parameter d_{12}. The influence of cross-diffusion on system (4) is studied here. Several values of the parameters are given in Table 7. The value of the cross-diffusion parameter d_{12} is

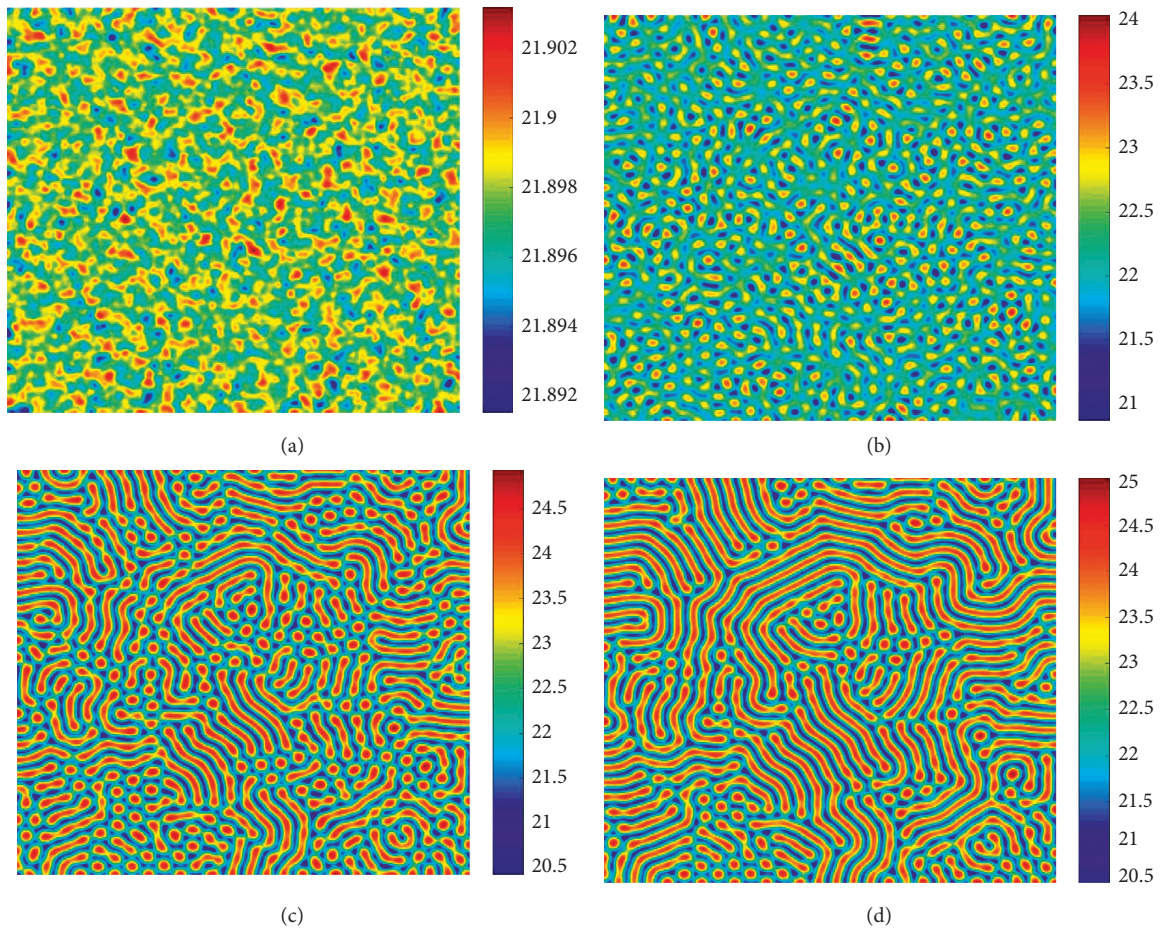

Figure 4: Iterations of the mixture of hot spots and stripes of the predator with $\gamma = 0.0118$; the other parameters are set as in Table 4. Iterations: (a) 0, (b) 15,000, (c) 50,000, and (d) 100,000.

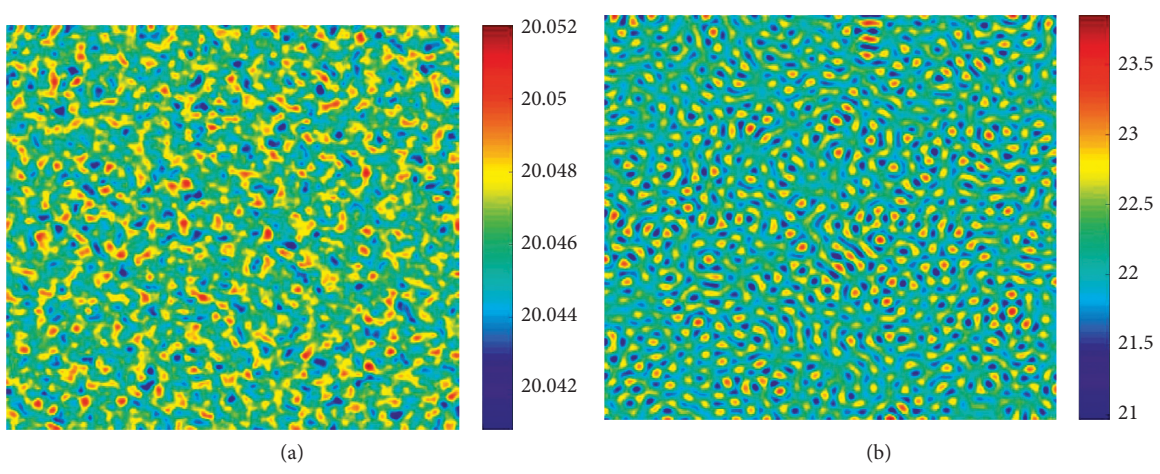

Figure 5: Continued.

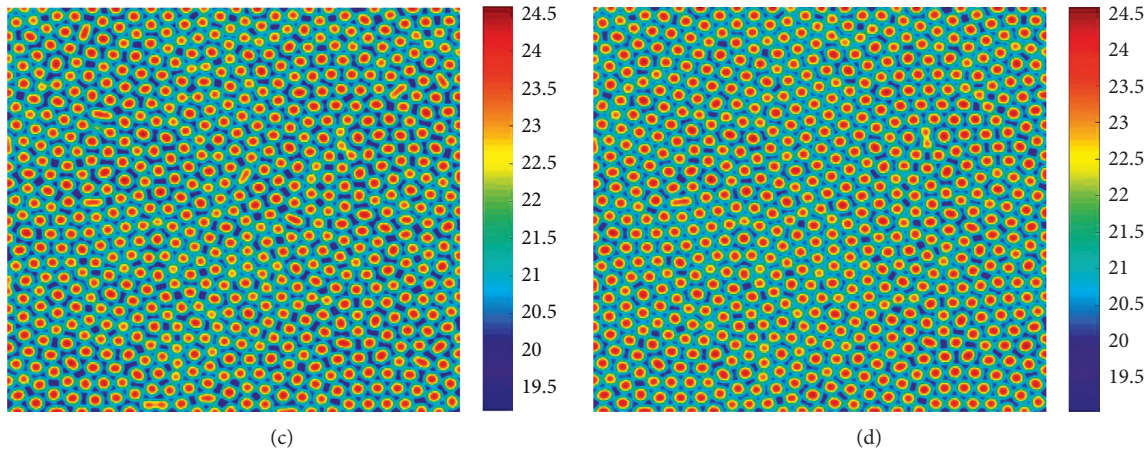

Figure 5: Iterations of hot spot pattern of the predator with $\gamma = 0.0105$; other parameters are set as in Table 4. Iterations: (a) 0, (b) 20,000, (c) 30,000, and (d) 100,000.

Table 6: Parameters set in system (4).

η	e	d_{11}	d_{22}	d_{12}	d_{21}
0.8	130	0.1	8.5	0.008	−0.08

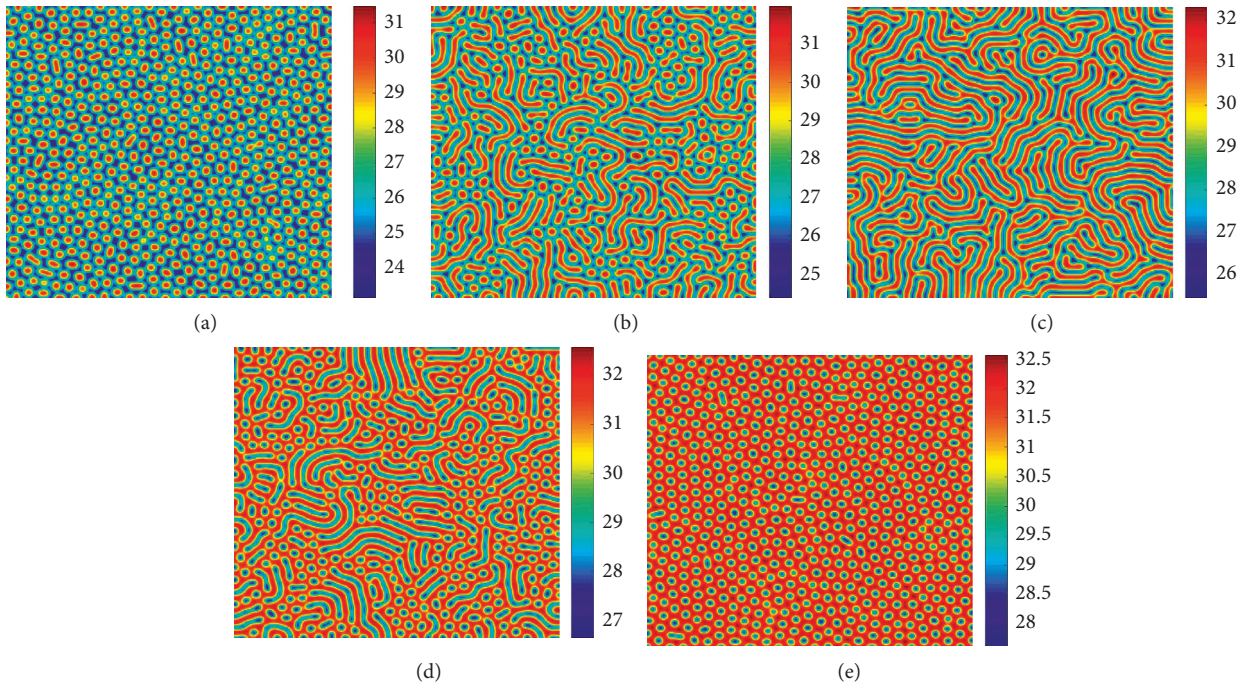

Figure 6: Spatial patterns of the predator induced by conversion rate of prey into predator biomass; other parameters are set as in Table 5. (a) $\gamma = 0.007041633659$, (b) $\gamma = 0.008509501103$, (c) $\gamma = 0.009332994621$, (d) $\gamma = 0.01032204568$, and (e) $\gamma = 0.01092704597$.

decreased. When fixing d_{12} as 0.01, the spot pattern shown in Figure 7(a) can be simulated. When d_{12} decreases to 0.006, the mixture of hot spots and stripes emerges, as shown in Figure 7(b). In Figure 7(c), a stripe pattern arises as d_{12} further decreases to 0.004. Finally, the entire spatial domain is filled in with cold spots and stripes when d_{12} is chosen only as 0.001. Figure 7 shows the regular changes of the pattern transition with the density of the prey increasing from 0.5 to 0.6 gradually as the value of d_{12} decreases. 12 is the cross-diffusion rate of the prey when the prey species encounters the predator. In other words, the larger the value of 12, the greater the chance that the prey will encounter the predator; that is, the prey will be at greater risk of being eaten by the predator as the prey's population decreases. This result has a clear biological meaning.

Table 7: Parameters set in system (4).

η	e	γ	d_{11}	d_{22}	d_{21}
0.8	530	0.00204801456	0.2	12	−0.074

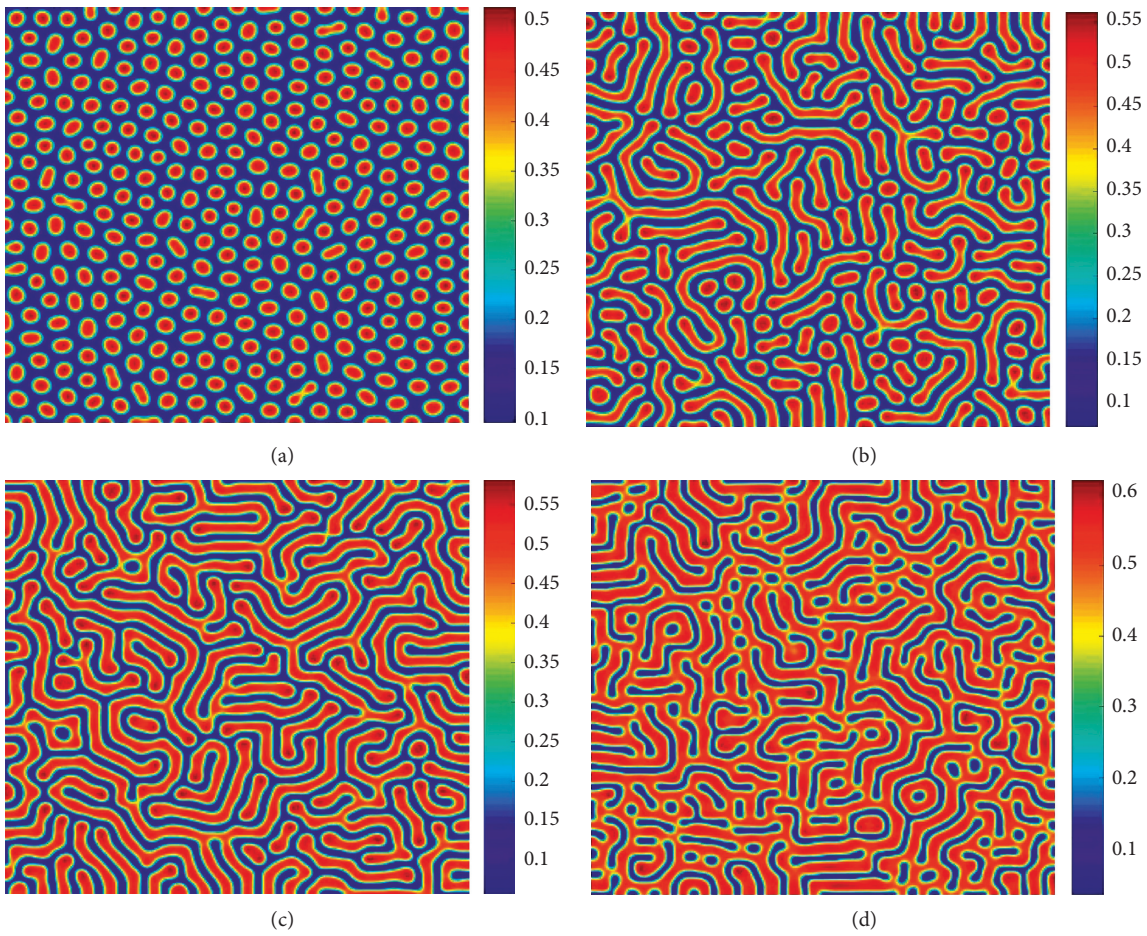

Figure 7: Spatial patterns of prey induced by cross-diffusion. (a) $d_{12} = 0.01$, (b) $d_{12} = 0.006$, (c) $d_{12} = 0.004$, and (d) $d_{12} = 0.001$.

5. Conclusion and Discussion

A prey-predator model of Holling–Tanner type with cross-diffusion was studied. Pattern selection and formation of the model were analyzed via weakly multiple scale analysis. First, the condition for the Turing instability of the model was obtained. Then, by choosing γ as a bifurcation parameter, the amplitude equations were deduced and the Turing pattern selection of model (4) presented. The theoretical analysis was verified by numerical results, as follows: An unstable H_π spot pattern, unstable mixture of cold spots and stripes, and unstable stripe pattern appear, when μ satisfies $\mu_2 < \mu = 0.0068256080 < \mu_3$, $\mu_2 < \mu = 0.0290608556 < \mu_3$ and $\mu_2 < \mu = 0.1031783475 < \mu_3$, respectively. The stable mixture of spots and stripes arises when $\mu_3 < \mu = 0.1254135951 < \mu_4$ holds. Finally, it was found that the conversion of biomass from prey to predator, as well as cross-diffusion, can also result in the transition of the patterns. Compared with [9], we not only computed the interval of pattern selection mathematically, but also obtained the Turing pattern corresponding with the interval. Moreover, we studied the prey-predator model of Holling–Tanner type with cross-diffusion explosively, from aspects of pattern selection and the influence of the cross-diffusion and the intrinsic factor of conversion rate of biomass from prey to predator with rich numerical simulations.

Cross-diffusion terms explain the influence of the population density of one species on the movement of other species apart from random diffusion (i.e., self-diffusion) of both species. Our numerical results about pattern transitions of prey induced by parameter d_{12} reveal that the more frequent the prey moves, the greater chance the prey will be at greater risk of population decreasing. This helps us further understand the cross-diffusion induced change of dynamics. Besides, together with our results about pattern transitions of the predator induced by parameter conversion rate of biomass from prey to predator, which is an intrinsic factor of prey-predator model, our study indicates that the real intrinsic mutual influence between prey and predator, along with the inherent mechanism of cross-diffusion, dominates

the persistence or extinction of the entire biological system [48]. Our results are general in nature and can be used to study the effect of cross-diffusion on other prey-predator models both analytically and numerically. However, we mainly consider pattern transitions of prey induced by parameter d_{12}. Similarly, we can study pattern transitions of prey induced by the other cross-diffusion parameter d_{21} and compare the differences between pattern transitions induced by d_{12} and d_{21} in our future study. Besides, we chose γ as the control parameter because γ is the parameter that stands for apparent relationship between the predator and prey. We can also choose another parameter as the control parameter to investigate the pattern transition in our future work.

Multiple scale analysis around the Turing bifurcation is used to analyze the stability of different Turing patterns via the amplitude equations. Our study gets the intervals for the pattern selection. These results have been validated numerically and they matched the theoretical analysis to a large extent. Linear analysis is to analyze Turing bifurcation and Turing domain. Compared with the linear analysis, multiple scale analysis is to analyze the dynamical behavior of our model in detail (i.e., pattern selection). However, one should be aware that pattern selection is only meaningful when the value of the controlled parameter is selected to be close to the threshold of γ_T. Moreover, the method of the multiple scale analysis may be applied in spatial epidemic models in the future to gain further insight into the extinction and persistence of a disease [49, 50]. Furthermore, we can take into account the imprecise value of the parameter and study the Turing patterns of an imprecise prey-predator model in future study.

Data Availability

All data and models generated or used during the study appear in the submitted article.

Conflicts of Interest

The authors declare that they have no conflicts of interest.

Acknowledgments

This work was supported by the Youth Science and Technology Research Foundation of Shanxi Province (Grant No. 201801D221033), Scientific Research Project of Xinzhou Teachers University (2019KY07), and Key Construction Disciplines Project of Xinzhou Teachers University (XK201501).

References

[1] J. D. Murray, "Spatial structures in predator-prey communities- a nonlinear time delay diffusional model," *Mathematical Biosciences*, vol. 31, no. 1-2, pp. 73–85, 1976.

[2] J. Guckenheimer, G. Oster, and A. Ipaktchi, "The dynamics of density dependent population models," *Journal of Mathematical Biology*, vol. 4, no. 2, pp. 101–147, 1977.

[3] R. Arditi, J. M. Abillon, and J. D. S. Vieira, "A predator-prey model with satiation and intraspecific competition," *Ecological Modelling*, vol. 5, no. 3, pp. 173–191, 1978.

[4] A. J. Lotka, *Elements of Physical Biology*, Williams and Wilkins Company, Baltimore, USA, 1925.

[5] V. Volterra, "Fluctuations in the abundance of a species considered Mathematically1," *Nature*, vol. 118, no. 2972, pp. 558–560, 1926.

[6] J. L. Lv, X. L. Zou, and L. H. Tian, "A geometric method for asymptotic properties of the stochastic Lotka-Volterra model," *Communications in Nonlinear Science and Numerical Simulation*, vol. 67, pp. 449–459, 2018.

[7] M. E. Gilpin, "A model of the predator-prey relationship," *Theoretical Population Biology*, vol. 5, no. 3, pp. 333–344, 1974.

[8] Q. Xue, G. Q. Sun, C. Liu et al., "Spatiotemporal dynamics of a vegetation model with nonlocal delay in semi-arid environment," *Nonlinear Dynamics*, vol. 99, no. 4, pp. 3407–3420, 2020.

[9] G. Q. Sun, S. L. Wang, Q. Ren, Z. Jin, and Y. P. Wu, "Effects of time delay and space on herbivore dynamics: linking inducible defenses of plants to herbivore outbreak," *Scientific Reports*, vol. 11246, 2014.

[10] G. Q. Sun, C. H. Wang, L. L. Chang, Y. P. Wu, L. Li, and Z. Jin, "Effects of feedback regulation on vegetation patterns in semi-arid environments," *Applied Mathematical Modelling*, vol. 61, pp. 200–215, 2018.

[11] G. Q. Sun, C. H. Wang, and Z. Y. Wu, "Pattern dynamics of a Gierer-Meinhardt model with spatial effects," *Nonlinear Dynamics*, vol. 88, no. 2, pp. 1385–1396, 2017.

[12] J. Li, G. Q. Sun, and Z. Jin, "Pattern formation of an epidemic model with time delay," *Physica A: Statistical Mechanics and Its Applications*, vol. 403, pp. 100–109, 2014.

[13] Z. G. Guo, L. P. Song, G. Q. Sun, C. Li, and Z. Jin, "Pattern dynamics of an SIS epidemic model with nonlocal delay," *Int J Bifurcation Chaos*, vol. 29, no. 2, 2019.

[14] M. Banerjee, S. Ghorai, and N. Mukherjee, "Study of cross-diffusion induced Turing patterns in a ratio-dependent prey-predator model via amplitude equations," *Applied Mathematical Modelling*, vol. 55, pp. 383–399, 2018.

[15] N. Mukherjee and V. Volpert, "Bifurcation scenario of Turing patterns in prey-predator model with nonlocal consumption in the prey dynamics," *Communications in Nonlinear Science and Numerical Simulation*, vol. 96, Article ID 105677, 2021.

[16] S. Mishra, "Population dynamic consequences of fearful prey in a spatiotemporal predator-prey system," *Mathematical Biosciences and Engineering*, vol. 16, no. 1, pp. 338–372, 2019.

[17] S. Yuan, C. Xu, and T. Zhang, "Spatial dynamics in a predator-prey model with herd behavior," *Chaos*, vol. 23, Article ID 033102, 2013.

[18] Y. F. Jia, Y. L. Cai, H. B. Shi, S. M. Fu, and W. M. Wang, "Turing patterns in a reaction–diffusion epidemic model," *International Journal of Biomathematics*, vol. 11, no. 2, 2018.

[19] J. P. Tripathi, S. Abbas, G. Q. Sun, D. Jana, and C. H. Wang, "Interaction between prey and mutually interfering predator in prey reserve habitat: pattern formation and the Turing-Hopf bifurcation," *Journal of the Franklin Institute*, vol. 355, no. 15, pp. 7466–7489, 2018.

[20] J. Li, Z. Jin, and G. Q. Sun, "Periodic solutions of a spatio-temporal predator-prey system with additional food," *Chaos, Solitons & Fractals*, vol. 91, pp. 350–359, 2016.

[21] P. H. Leslie, "Some further notes on the use of matrices in population mathematics," *Biometrika*, vol. 35, no. 3-4, pp. 213–245, 1948.

[22] M. P. Hassell, *The Dynamics of Arthropod Predator–Prey Systems*, Princeton University Press, Princeton, NJ, USA, 1978.

[23] C. S. Holling, "The functional response of predators to prey density and its role in mimicry and population regulation," *Memoirs of the Entomological Society of Canada*, vol. 97, no. S45, pp. 5–60, 1965.

[24] P. A. Braza, "The bifurcation structure of the holling--tanner model for predator-prey interactions using two-timing," *SIAM Journal on Applied Mathematics*, vol. 63, no. 3, pp. 889–904, 2003.

[25] J. T. Tanner, "The stability and the intrinsic growth rates of prey and predator populations," *Ecology*, vol. 56, no. 4, pp. 855–867, 1975.

[26] D. Wollkind, J. Collings, and J. Logan, "Metastability in a temperature-dependent model system for predator-prey mite outbreak interactions on fruit trees," *Bulletin of Mathematical Biology*, vol. 50, no. 4, pp. 379–409, 1988.

[27] Y. Huang, F. Chen, and L. Zhong, "Stability analysis of a prey-predator model with holling type III response function incorporating a prey refuge," *Applied Mathematics and Computation*, vol. 182, no. 1, pp. 672–683, 2006.

[28] J. H. P. Dawes and M. O. Souza, "A derivation of Holling's type I, II and III functional responses in predator-prey systems," *Journal of Theoretical Biology*, vol. 327, pp. 11–22, 2013.

[29] G. Q. Sun, "Mathematical modeling of population dynamics with Allee effect," *Nonlinear Dynamics*, vol. 85, no. 1, pp. 1–12, 2016.

[30] E. H. Kerner, "A statistical mechanics of interacting biological species," *Bulletin of Mathematical Biophysics*, vol. 19, no. 2, pp. 121–146, 1957.

[31] Y. Cai and W. Wang, "Stability and Hopf bifurcation of the stationary solutions to an epidemic model with cross-diffusion," *Computers & Mathematics with Applications*, vol. 70, no. 8, pp. 1906–1920, 2015.

[32] A. Madzvamuse, H. S. Ndakwo, and R. Barreira, "Cross-diffusion-driven instability for reaction-diffusion systems: analysis and simulations," *Journal of Mathematical Biology*, vol. 70, no. 4, pp. 709–743, 2015.

[33] W. Abid, R. Yafia, M. A. A. Alaoui, and A. Aghriche, "Turing instability and Hopf bifurcation in a modified Leslie-Gower predator-prey model with cross-diffusion," *Int J Bifurcation Chaos*, vol. 28, 2018.

[34] D. Horstmann, "Remarks on some Lotka-Volterra type cross-diffusion models," *Nonlinear Analysis: Real World Applications*, vol. 8, no. 1, pp. 90–117, 2007.

[35] C. Wang and S. Qi, "Spatial dynamics of a predator-prey system with cross diffusion," *Chaos, Solitons & Fractals*, vol. 107, pp. 55–60, 2018.

[36] R. R. Baier and C. Tian, "Mathematical analysis and numerical simulation of pattern formation under cross-diffusion," *Nonlinear Analysis: Real World Applications*, vol. 14, no. 1, pp. 601–612, 2013.

[37] E. E. Holmes, M. A. Lewis, J. E. Banks, and R. R. Veit, "Partial differential equations in ecology: spatial interactions and population dynamics," *Ecology*, vol. 75, no. 1, pp. 17–29, 1994.

[38] Y. Cai and W. Wang, "Fish-hook bifurcation branch in a spatial heterogeneous epidemic model with cross-diffusion," *Nonlinear Analysis: Real World Applications*, vol. 30, pp. 99–125, 2016.

[39] T. Zhang, Y. Xing, H. Zang, and M. Han, "Spatio-temporal dynamics of a reaction-diffusion system for a predator-prey model with hyperbolic mortality," *Nonlinear Dynamics*, vol. 78, no. 1, pp. 265–277, 2014.

[40] W. Wang, Y. Lin, L. Zhang, F. Rao, and Y. Tan, "Complex patterns in a predator-prey model with self and cross-diffusion," *Communications in Nonlinear Science and Numerical Simulation*, vol. 16, no. 4, pp. 2006–2015, 2011.

[41] R. Peng, M. Wang, and G. Yang, "Stationary patterns of the Holling-Tanner prey-predator model with diffusion and cross-diffusion," *Applied Mathematics and Computation*, vol. 196, no. 2, pp. 570–577, 2008.

[42] K. Oeda, "Effect of cross-diffusion on the stationary problem of a prey-predator model with a protection zone," *Journal of Differential Equations*, vol. 250, no. 10, pp. 3988–4009, 2011.

[43] L. Chang, G. Q. Sun, Z. Wang, and Z. Jin, "Rich dynamics in a spatial predator-prey model with delay," *Applied Mathematics and Computation*, vol. 256, pp. 540–550, 2015.

[44] V. Tiwari, J. P. Tripathi, S. Abbas, J. S. Wang, G. Q. Sun, and Z. Jin, "Qualitative analysis of a diffusive Crowley-Martin predator-prey model: the role of nonlinear predator harvesting," *Nonlinear Dynamics*, vol. 98, no. 2, pp. 1169–1189, 2019.

[45] Q. Ouyang, *Patterns Formation in Reaction–Diffusion Systems*, Shanghai Sci.-Tech. Education Publishing House, Shanghai, China, 2000.

[46] C. Wang, L. Chang, and H. Liu, "Spatial patterns of a predator-prey system of Leslie type with time delay," *PLoS One*, vol. 11, Article ID e0150503, 2016.

[47] T. D. Frank, "Formal derivation of Lotka–Volterra–Haken amplitude equations of taskrelated brain activity in multiple, consecutively performed tasks," *International Journal of Bifurcation and Chaos*, vol. 26, 2016.

[48] G. Q. Sun, Z. Y. Wu, Z. Wang, and Z. Jin, "Influence of isolation degree of spatial patterns on persistence of populations," *Nonlinear Dynamics*, vol. 83, no. 1-2, pp. 811–819, 2016.

[49] G. Q. Sun, M. Jusup, Z. Jin, Y. Wang, and Z. Wang, "Pattern transitions in spatial epidemics: mechanisms and emergent properties," *Physics of Life Reviews*, vol. 9, pp. 74-75, 2016.

[50] Z. G. Guo, G. Q. Sun, Z. Wang, Z. Jin, and C. Li, "Spatial dynamics of an epidemic model with nonlocal infection," *Applied Mathematics and Computation*, vol. 377, Article ID 125158, 2020.